Microstructure and fatigue properties of a friction stir lap welded magnesium alloy

Naik, B.S.; Chen, D.L.; Cao, X.; Wanjara, P.

National Research Council Canada   Conseil national de recherches Canada

Canada

Microstructure and Fatigue Properties of a Friction Stir Lap Welded Magnesium Alloy

B.S. NAIK, D.L. CHEN, X. CAO, and P. WANJARA

Friction stir welding (FSW), being an enabling solid-state joining technology, can be suitably applied for the assembly of lightweight magnesium (Mg) alloys. In this investigation, friction stir lap welded (FSLWed) joints of AZ31B-H24 Mg alloy were characterized in terms of the welding defects, microstructure, hardness, and fatigue properties at various combinations of tool rotational rates and welding speeds. It was observed that the hardness decreased from the base metal (BM) to the stir zone (SZ) across the heat-affected zone (HAZ) and thermomechanically affected zone (TMAZ). The lowest value of hardness appeared in the SZ. With increasing tool rotational rate or decreasing welding speed, the average hardness in the SZ decreased owing to increasing grain size, and a Hall–Petch-type relationship was established. Fatigue fracture of the lap welds always occurred at the interface between the SZ and TMAZ on the advancing side where a larger hooking defect was present (in comparison with the retreating side). The welding parameters had a significant influence on the hook height and the subsequent fatigue life. A relatively "cold" weld, conducted at a rotational rate of 1000 rpm and welding speed of 20 mm/s, gave rise to almost complete elimination of the hooking defect, thus considerably (over two orders of magnitude) improving the fatigue life. Fatigue crack propagation was basically characterized by the formation of fatigue striations concomitantly with secondary cracks.

I. INTRODUCTION

THE growing environmental concern about global climate change in conjunction with highly volatile and rising energy prices has resulted in continuous and increasing pressure on the transportation industry to improve fuel efficiency and reduce anthropogenic environment-damaging emissions.[1–7] Different strategies can be employed to address this challenge, including the use of alternative/renewable energy sources and the related powertrain improvements, aerodynamic (drag reducing) enhancements, and vehicle lightweighting. Of these, reduction of vehicle weight has been the preferred approach in the global transportation industry. In principle, material selection strategies for vehicle components and assemblies are dependent on functionality, cost, lightweighting, and recyclability considerations.[1,8–17] Substitution of traditional materials, such as mild steels, for example, with advanced high-strength steels or aluminum alloys, has already allowed marked gains in weight reduction and there is further potential through judicious application of ultralightweight Mg alloys.[18] Of importance for realizing increased use of Mg alloys for lightweighting is the development of cost-effective joining technologies that render the high mechanical performance of the assembly.

Mg alloys may be welded using conventional arc and advanced fusion (e.g., laser) welding techniques. However, these processes tend to require filler metal addition to mitigate weld cracking through modification of the molten weld pool composition as well as post-weld heat treatment to restore the fusion zone strength in hardened alloys.[19,20] Other challenges for fusion welding of Mg stem from its relatively low viscosity and surface tension in the molten state, high oxidation potential,[21] relatively high vapor pressure in the liquid phase, and significantly high hydrogen solubility in the liquid phase relative to the solid phase,[22,23] which can result in an unstable weld pool, production of spatter, poor surface quality, porosity, solid inclusions, and evaporative losses (especially for the elements with high evaporative pressures and low boiling points such as zinc).[24] Therefore, the applications of lightweight Mg alloys require the development and application of alternative advanced welding technologies, while guaranteeing the reliability and structural integrity of the welded joints.

Friction stir welding (FSW), an emerging "green" solid-state joining process that was invented at The Welding Institute (TWI) of UK in 1991,[8] can mitigate the above concerns linked to the melting and solidification of the weldment to render mechanical performance improvements for the assembly because the Mg alloy does not reach its melting temperature. Utilization of

B.S. NAIK, Ph.D. Student, and D.L. CHEN, Professor and Ryerson Research Chair, are with the Department of Mechanical and Industrial Engineering, Ryerson University, Toronto, ON M5B 2K3, Canada. Contact e-mail: dchen@ryerson.ca X. CAO, Senior Research Officer, and P. WANJARA, Group Leader, are with the National Research Council Canada Aerospace, 5145 Decelles Avenue, Montreal, Quebec H3T 2B2, Canada

FSW can be especially advantageous for Mg alloys as the process imparts a low heat input and has the flexibility to join cast, extruded, and rolled materials without requiring complicated surface preparation or shielding gas protection.[25,26] FSW can also assemble different joint configurations, such as lap, butt, and T-joints, of which the lap joints are widely applied in vehicle and aircraft design and manufacturing. Of importance for friction stir lap welding (FSLW), however, is the greater diligence necessary in developing and optimizing tool designs and process parameters to break the surface oxide layer on two planar surfaces and mitigate the three main defects, *i.e.*, kissing bonds, hooking, and top workpiece thinning.[27]

While a number of studies have been conducted on FSLW of Al alloys in the last decade, work reported on the FSLW of Mg alloys is rather limited. Specifically, Cao and Jahazi[16,28] studied the FSLW of AZ31B-H24 Mg alloy to identify the effect of welding speed and tool rotational rate on lap joint quality and determined a hardness trough in the weldment that diminished slightly at a low tool rotational rate and high welding speed. Yang *et al.*[29] investigated the effect of different tool geometries (*i.e.*, a concave shoulder with a cylindrical-, triangular-, or pie-shaped pin) and process conditions on the weld quality and static lap shear strength of the AZ31B-H24 Mg alloy; a strong dependence of the lap shear strength on the hook height was observed with a joint efficiency of the welds ranging between 68 and 76 pct of the tensile strength of base metal (BM). With regard to the fatigue properties, to the authors' knowledge, no such work on the behavior of FSLWed Mg alloy assemblies is available in the open literature. For Al alloys, the limited information on the lap welded joints has indicated that the welding defects, such as hooking and the redistribution of the unwelded lap oxide layers,[30] can reduce the effective thickness of the top workpiece and orient the unwelded lap as a pre-crack to a more preferred crack propagation direction, significantly reducing the fatigue properties.[17,31,32] Considering that fatigue performance is crucial for dynamic loading design of materials and structural integrity and safety, the present investigation aimed to study the effect of the FSLW process parameters on the weld integrity, microstructure, hardness, and fatigue properties of AZ31B-H24 Mg alloy.

II. EXPERIMENTAL PROCEDURE

The BM selected in this study was a 2-mm-thick AZ31B-H24 Mg alloy in the sheet form with dimensions of 1200 mm × 500 mm and a nominal composition (wt pct) of 2.5-3.5 Al, 0.7-1.3 Zn, 0.2-1.0 Mn, and the balance Mg. Test coupons, 300 mm (length) × 100 mm (width), were sectioned from the as-received sheets followed by milling of the edges along the length. Surface preparation of the sheets prior to FSLW consisted of cleaning the faying surfaces and the surrounding areas with ethanol, followed by scouring with an abrasive pad to remove the oxides, and final cleaning in ethanol. The workpieces were then over-

lapped with a width of approximately 28 mm, as indicated in Figures 1(a) and (b), and tightly clamped using spacers within a welding fixture that was secured to the backing anvil/worktable of an ISTIR MTS FSW system. FSLW was conducted in the position control mode using a H13 steel tool (46.6–50 HRC) that consisted of a scrolled shoulder with a diameter of 19.05 mm and an adjustable ¼-20 left-hand threaded pin having a diameter of 6.35 mm, a threaded length of 4.45 mm, a thread spacing of 1.27 mm, and a pitch of 0.8 thread/mm. The tool-to-workpiece angle was maintained at 0.5 deg with a shoulder heel plunge depth (the portion of the shoulder under the top surface of the workpiece) of approximately 0.25 mm for all the welding experiments. The welding direction was perpendicular to the rolling direction of the workpiece (Figure 1(c)) and all the joints were FSLWed at a speed of 10 mm/s or 20 mm/s. The tool rotational rates were 1000 rpm and 1500 rpm at a pin length of 2.75 mm. It is noteworthy that relative to the welding and tool rotational directions indicated in Figure 1, the welds were manufactured with the retreating side (RS) near the edge of the top workpiece, abbreviated as RNE.

The weld integrity was characterized in terms of the welding defects, microstructure, hardness, and fatigue properties. For each FSLWed assembly, the unstable (ramp up and ramp down) regions at the beginning (~50 mm) and end (~20 mm) of the weld were removed. Using a diamond wafering blade on a slow-speed cutoff saw, the FSLWed assemblies were sectioned in the direction perpendicular to the welding direction (WD) to examine the microstructures in the weld cross sections. Sectioned coupons were then cold mounted, ground, polished, and etched with acetic picral [10 mL acetic acid (99 pct), 4.2 g picric acid, 10 mL H_2O, and 70 mL ethanol (95 pct)] for approximately 6 seconds to reveal the grain structure. Microstructural analysis was carried out using an optical microscope equipped with quantitative image analysis software. Automated Vickers microindentation hardness testing was conducted across the lap welds at the mid-thickness of the top and bottom workpieces using a load of 100 g, a dwell time of 15 seconds, and an indent interval of 0.3 mm (*i.e.*, at least three times the diagonal length of the indentation to prevent any potential effect of the strain fields caused by adjacent indentations).

For each welded assembly, two tensile-shear specimens were cut using an abrasive waterjet micromachining system to obtain a specimen width of 20 mm (Figure 1(c)), according to ASTM D3164,[33] and an overall joint length of approximately 160 mm. To balance the offset axes of the lap members and minimize bending effects, two spacers having the same thickness as the workpieces (*i.e.*, 2 mm) were used during the fatigue tests, as illustrated in Figure 1(d). Considering the RNE configuration, during tensile-shear testing, the advancing side (AS) of the lap weld on the upper member was loaded (Mode I). Fatigue tests were performed using a fully computerized Instron 8801 servo-hydraulic testing system under load control. Before fatigue testing, all the lateral edges of the fatigue specimens were slightly ground using abrasive papers up
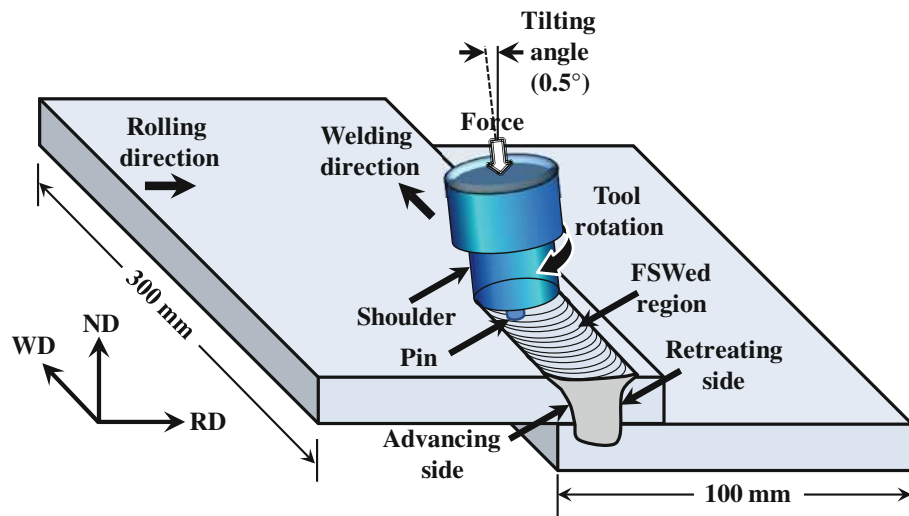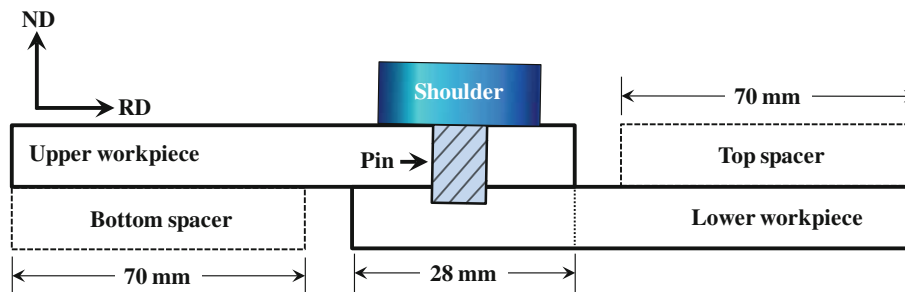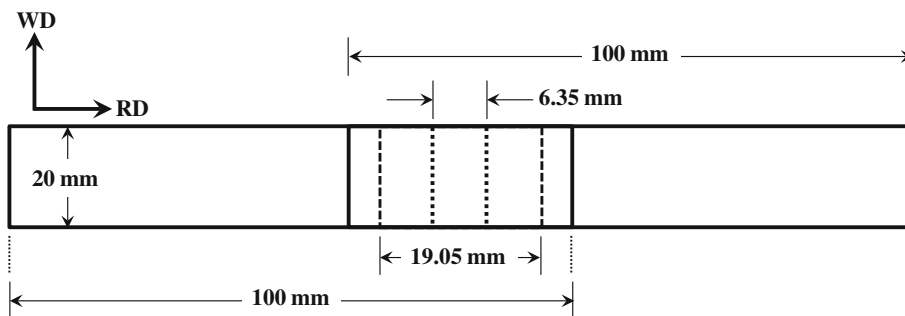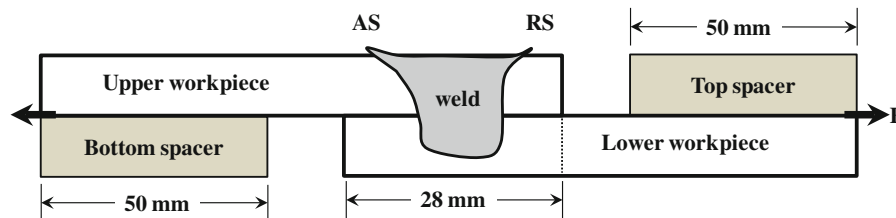
Fig. 1—Schematic diagrams of the experimental setup showing (*a*) the friction stir lap welding process, (*b*) the side view of the overlapped Mg/Mg joint, (*c*) the top view of the welded coupon, and (*d*) the setup for fatigue testing (Mode I).

to a grit number of 600, so as to avoid the influence of local surface stress concentration. A load ratio R (= P_{min}/P_{max}) set at 0.2, a sinusoidal waveform, and a frequency of 50 Hz were applied during the fatigue tests. The stress was calculated as the applied load divided by the specimen cross-sectional area

(2 mm × 20 mm) according to References 31, 34. At least two samples were tested at each load level. All mechanical tests were performed up to failure. The fracture surface of the friction stir lap welds after fatigue testing was examined using a JSM-6380LV scanning electron microscope (SEM) equipped with an Oxford energy dispersive X-ray spectroscopy (EDS) system with three-dimensional (3D) fractographic analysis capacity.

III. RESULTS AND DISCUSSION

A. Welding Defects

Figure 2 shows macroscopic overviews of the lap welds obtained at various tool rotational rates and welding speeds with a pin length of 2.75 mm. According to the relationship between the tool rotational direction and welding direction, two sides can be identified: the AS and the RS that correspond to the left- and right-hand sides in Figure 2. On both the AS and RS, defects such as hooking and kissing bonds were observed. Overall, the hooking defect, which was normally observed at a lower magnification, was most evident at

the TMAZ of the AS in the AZ31B-H24 Mg alloy lap welds, where the interface of the workpieces was pulled up into the top workpiece. Also, the hook was inclined upward toward the weld surface and terminated at the border of the SZ. In the AZ31B-H24 Mg alloy lap welds, the kissing bond defects (to be discussed below) were a result of insufficient mixing at the interface of the workpieces that led to the presence of separated interfaces with entrained oxide layers. It is noteworthy that the kissing bonds have recently been deliberated to be more suitably referred to as the "Original Joint Line with Severe Plastic Deformation (OJLwSPD)."[35]

As the hooking defect causes the local thinning of the effective sheet thickness (EST) for the top or bottom workpiece and subsequently decreases the load-bearing capacity or strength of the joint, understanding the effect of the tool rotational rate and welding speed on the relative size of the hook defects is important. In particular, the tool rotational rate was observed to have a significant influence on the formation of hooking defects, as indicated in Figure 3, with a decrease from 1500 rpm to 1000 rpm resulting in considerable reduction in the hook height from ~1.4 mm to ~0.14 mm on
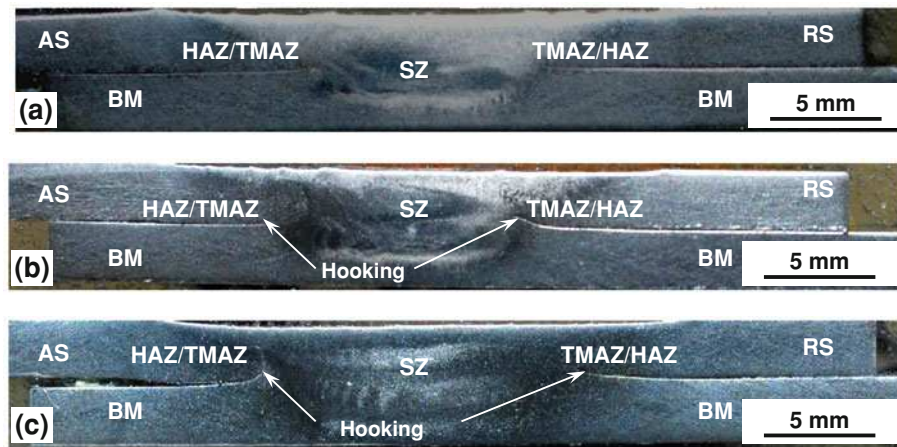

Fig. 2—Macroscopic images of the lap joints obtained at various combinations of rotational rate and welding speed of (a) 1000 rpm, 20 mm/s, (b) 1500 rpm, 20 mm/s, and (c) 1500 rpm, 10 mm/s.
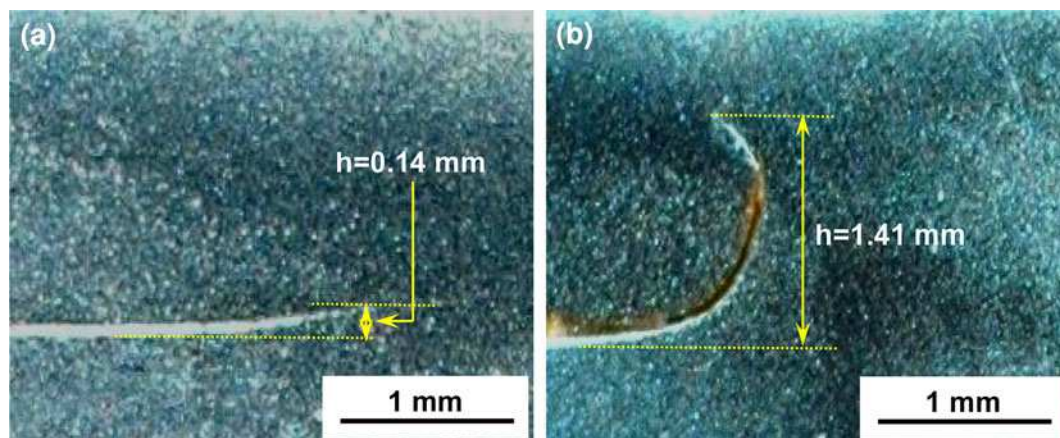

Fig. 3—Hooking defects in the friction stir lap welds and their relative sizes on the AS for the welding conditions of (a) 1000 rpm at 20 mm/s and (b) 1500 rpm at 20 mm/s.
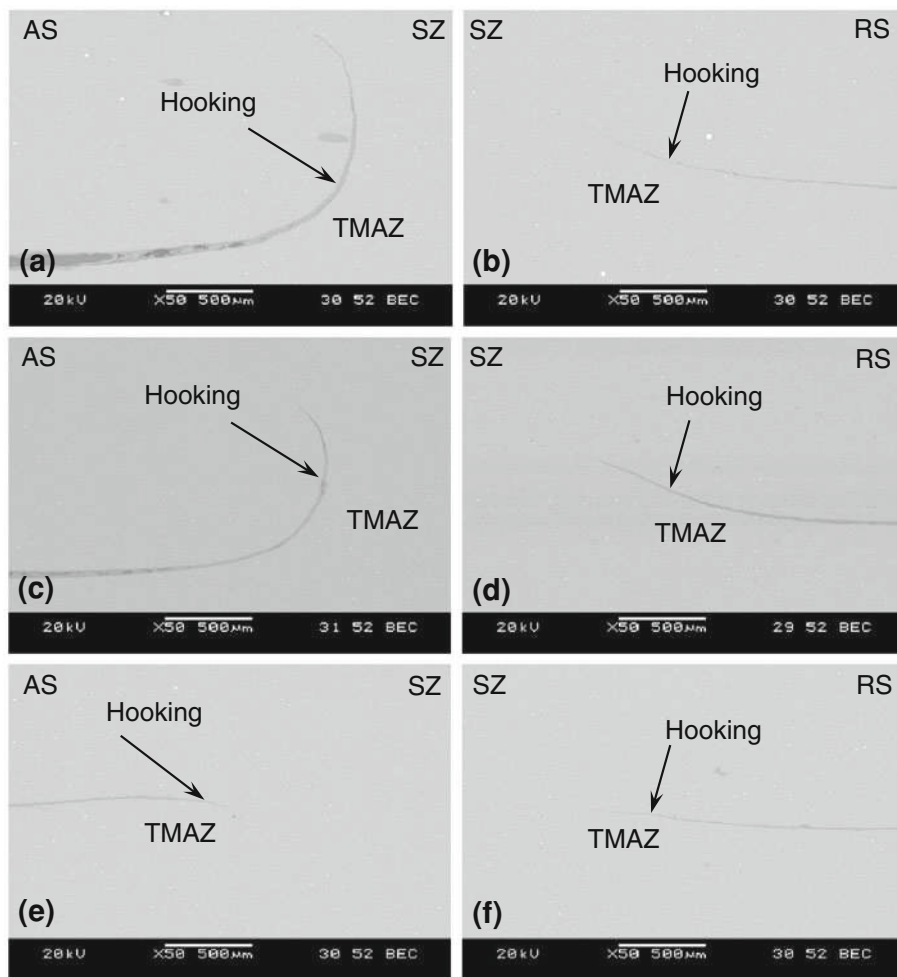
Fig. 4—Hooking defects observed on the advancing (left) and retreating (right) sides at varying tool rotational rates and welding speeds, namely (a) to (b) 1500 rpm and 10 mm/s, (c) to (d) 1500 rpm and 20 mm/s, and (e) to (f) 1000 rpm and 20 mm/s.

the AS. The welding speed was observed to have a secondary effect on the hook size, as illustrated in the SEM images of the hooking defects on the AS and RS of the lap welds depicted in Figure 4. In general, the hook height on the AS decreased from ~1.4 mm to ~1.3 mm with increasing welding speed from 10 mm/s to 20 mm/s. A similar result for the FSLWed AZ31 Mg alloy was reported by Yang et al.[29]

These findings indicate that the material flow in the SZ, near either the AS or the RS, influences the characteristics of the hooking defect that appears in the TMAZ, i.e., the region surrounding the SZ, as observed in Figure 4. Specifically, with decreasing tool rotational rate or increasing welding speed, the heat input during FSW is reduced (to be discussed later). Also, within the weldment, severe deformation caused by the passage of the tool results in strain and heat gradients; the TMAZ experiences much lower plastic strain and temperature than the SZ. With due consideration of the results presented in Figures 3 and 4, the "cold" welding (low heat input) conditions were conducive to small hooking defects. It should be pointed out that the flow of the plasticized material during FSW is quite complicated as it is influenced by a variety of factors including tool thread

orientation, rotational direction, processing parameters, etc. Based on the analysis detailed in Reference 36, a left-hand threaded pin rotating clockwise would result in a downward flow of the material adjoining the pin surface and mitigate the formation of cavity defects at the bottom. This, however, would be further related to the combination of the rotational rate and the welding speed. A disproportionately high rotational rate or slow welding speed would push or drive an excessive amount of plasticized material toward the bottom, which then has to be squeezed out in the upward direction at a small distance from the pin surface, inevitably due to the constant volume process conditions during FSW. That is, the interfaces between the top and bottom workpieces, on both the AS and RS, would extend along the border between the SZ and TMAZ toward the upper tool shoulder. Similar observations that indicated material flow from the bottom into the top workpiece were reported in Reference 31. Increasing the tool rotational rate increases turbulent flow in the SZ and thereby exacerbates the hook size through a greater upward flow of the material in the TMAZ during FSLW. Similarly, decreasing the welding speed allows a more intense stirring action of the pin which promotes material
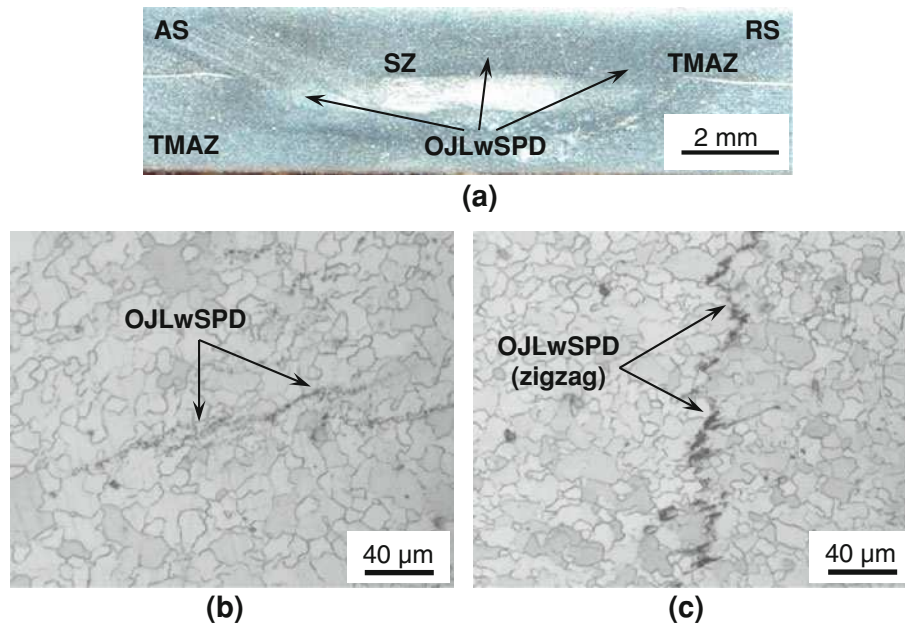
Fig. 5—(a) Low-magnification OJLwSPD defects present in between the top and bottom sheets of a weld joined at a welding speed of 20 mm/s and rotational rate of 1000 rpm using a pin of 2.75 mm in length; high-magnification observations of the OJLwSPD defects that occurred at a rotational rate of (b) 1000 rpm and (c) 1500 rpm.

movement upward. As the welding speed increases, the hooking defects may become progressively smaller, be completely eliminated, or even change their orientations as shown in Figures 4(e) and (f) for the AZ31B-H24 Mg alloy lap welds. Depending on the combination of rotational and welding speeds applied, the orientation of the hook on the AS may change significantly (sharply inclined upward to a slightly downward deflection (Figure 4(e)), while on the RS, the evolution is relatively gradual and remains inclined upward. Nonetheless, for each weld condition examined in the present study, the hook on the AS was not observed to interconnect to that from the RS or extend to the outer surface of the top/bottom workpiece.

Compared with the distinguishable hooking defects observed in the TMAZ, the kissing bonds or OJLwSPD defects usually appear as film-like, faint dark lines in the SZ (Figure 5). For the welding conditions in the present study, OJLwSPD defects with irregular morphologies, such as zigzag lines and wavy patterns, were observed in the SZ of each lap joint examined at a higher magnification and, in some cases, noted to extend throughout the SZ width (Figure 5). The recurrent oscillating traces of OJLwSPD, as shown in Figures 5(b) and (c), were associated with the formation of oxide bands.[37,38] Also, the OJLwSPD defects appearing in the SZ near the SZ/TMAZ interface may be an extension of the hooking defect in the TMAZ. However, the OJLwSPD defect width in the SZ was much narrower than that of the hooking defect in the TMAZ.

B. *Microstructure*

The thermomechanical conditions during FSLW of AZ31B-H24 Mg alloy resulted in the formation of distinct

regions in the weldment, namely the SZ or weld nugget around the weld centerline, the TMAZ on both sides of the SZ, and the HAZ surrounding the TMAZ and in turn delimited by the BM, as shown in Figure 6, where the typical microstructures were observed across a weld made at a welding speed of 20 mm/s and a rotational rate of 1000 rpm. The as-received microstructure of the BM consisted of mainly elongated/deformed grains in conjunction with fine equiaxed and recrystallized grains, as shown in Figure 6(g). This heterogeneous grain structure and size of the BM may originate from the incomplete dynamic recrystallization (partial annealing) during the warm rolling process as noted in Reference 28. At a higher resolution, mechanical twinning in the BM was also observed. In the SZ and TMAZ (Figures 6(c) to (e)), the severe plastic deformation and the elevated temperature resulted in dynamic recrystallization of the AZ31B-H24 Mg alloy, and the grains became predominately equiaxed in both regions. However, relative to the BM, the grains in the SZ and TMAZ were larger in size, indicating the concomitant occurrence of grain coarsening under the welding conditions in the present study. The HAZ microstructure lay in between those of TMAZ and BM. In comparison with the BM, the HAZ contained a greater fraction of equiaxed grains and a slightly coarser grain size due to the dominating effect of frictional heating, which resulted in the partial recrystallization of the elongated/deformed grains and the coarsening of the original equiaxed recrystallized grains in the BM microstructure in the H24 temper. This microstructural evolution observed in the different regions of the current friction stir lap welds of AZ31B-H24 Mg alloy is consistent with that appearing in the friction stir butt welds of AZ31B-H24 Mg alloy.[39–42]

The effect of the welding speed and tool rotational rate on the microstructure in the SZ is shown in
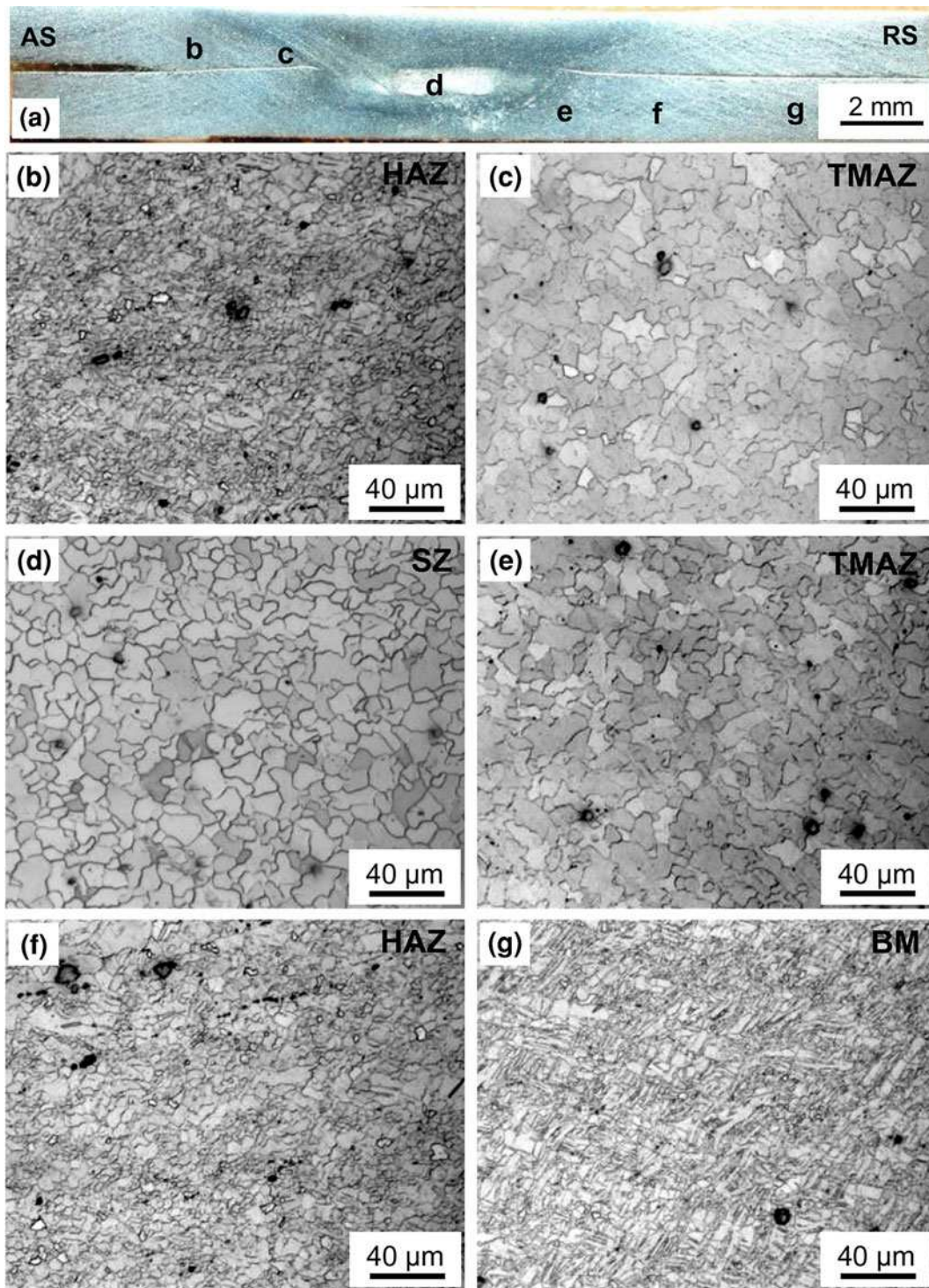
Fig. 6—(a) Overview of the FSLWed Mg/Mg joint obtained at a tool rotational rate of 1000 rpm and a welding speed of 20 mm/s with (b) to (g) showing the microstructures in the different regions as indicated in (a).

Figures 7(b) to (d) relative to the BM structure given in Figure 7(a). It is clear that the microstructure in the SZ was significantly different from that of the BM. At a constant welding speed of 20 mm/s, increasing the tool rotational rate from 1000 rpm to 1500 rpm was observed to increase the average grain size in the SZ from 7.4 μm to 8.6 μm. For the welding speed, a decrease from 20 mm/s to 10 mm/s at 1500 rpm resulted in a slight increase in the average grain size from 8.6 μm to 9.5 μm.

The increase in the average grain size observed with increasing tool rotational rate and decreasing welding speed is a result of the heat input that can be deliberated through the weld pitch (a ratio of the tool welding speed to the tool rotational rate). Specifically, a low weld pitch value of 0.4 mm/revolution for the combination of
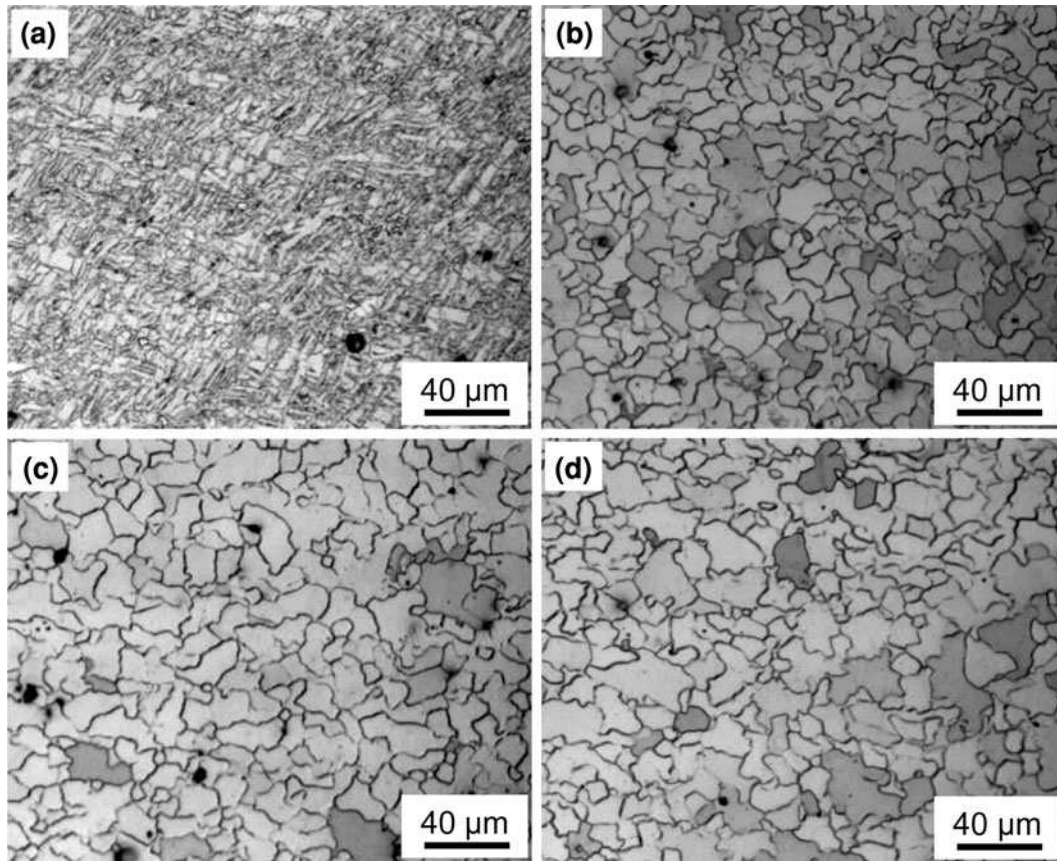
Fig. 7—Comparison of (*a*) the BM AZ31B-H24 Mg alloy microstructure with the typical microstructures in the SZ of FSLWed AZ31B-H24 Mg alloy at different tool rotational rates and welding speeds: (*b*) 1000 rpm and 20 mm/s, (*c*) 1500 rpm and 20 mm/s, and (*d*) 1500 rpm and 10 mm/s.

1500 rpm and 10 mm/s, which represents a ''hot'' welding condition, would render a coarse grain structure relative to a high weld pitch value of 1.2 mm/revolution or a ''cold'' welding condition at 1000 rpm and 20 mm/s. Alternatively, the effect of the welding parameters may be related to the heat input during FSW that has been given by Frigaard *et al.*[43] as follows:

$$q = \frac{4}{3}\pi^2 \mu P \omega R^3, \qquad [1]$$

where q is the heat input, μ is the friction coefficient, P is the pressure, ω is the tool rotational rate, and R is the radius of the shoulder. For a moving welding source, the heat input per unit length, Q, has been rewritten by Kim *et al.*[44] based on Eq. [1] as

$$Q \propto \frac{\alpha q}{v} = \frac{4}{3}\pi^2 \frac{\alpha \mu P \omega R^3}{v} \qquad [2]$$

where α is a heat input efficiency and v is the welding speed. When α, μ, and R are assumed to be constant, Eq. [2] can be simplified as

$$Q \propto \frac{P\omega}{v} = Pa \propto Fa \qquad [3]$$

where a is the ratio of the tool rotational rate to the welding speed (or the inverse of the weld pitch) and F is the tool plunge-down force. According to Eq. [3], at a constant welding speed (v), the heat input per unit length

(Q) increases linearly with increasing tool rotational rate (ω). Thus, a higher temperature in the SZ is expected at 1500 rpm than at the 1000 rpm condition, which explains the grain coarsening in the microstructure of the former (Figure 7(c)) with respect to the latter (Figure 7(b)) at a given welding speed of 20 mm/s. In contrast, at a constant rotational rate (ω), the heat input per unit length increases linearly with the inverse of the welding speed (v), and thus higher temperatures in the SZ are expected at 10 mm/s than at the 20 mm/s condition, which accounts for the coarser grain structure in the former (Figure 7(d)) microstructure relative to the latter (Figure 7(c)) at 1500 rpm.

C. *Microhardness*

Vickers microhardness profiles, measured at the mid-thickness in each workpiece across the AZ31B-H24 Mg alloy weldments assembled at different tool rotational rates and welding speeds, are given in Figures 8(a) to (c). For each welding condition, a hardness trough was observed with higher values in the BM relative to that in the TMAZ and SZ. The hardness decreased gradually from about 70–75 HV in the BM to approximately 55–62 HV at the center of the SZ of the welds, representing a decrease of up to ~25 pct. This hardness change was attributed to the effect of the welding parameters on the heat input during FSW and the resulting microstructural evolution (*i.e.*, average grain size) in the HAZ, TMAZ

and SZ, as depicted previously in Figures 6(b) to (d). Specifically, at a constant welding speed of 20 mm/s, an increase in the rotational rate from 1000 rpm to 1500 rpm was observed to decrease the average value of the hardness in the SZ from about 64 HV to about 54 HV (Figures 8(a) and (b)). As expected, this was due to the greater heat input and coarser SZ grain size in the latter welding condition, as seen in Figures 7(c) vs (b).

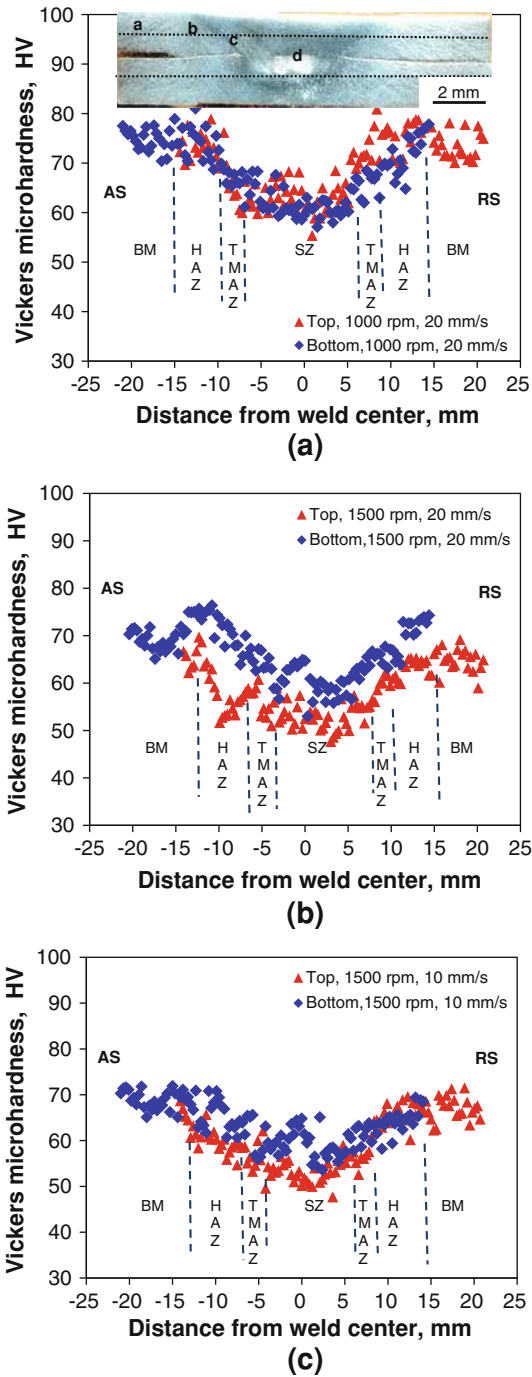**(a)**

(b)

(c)

Fig. 8—Typical microhardness profiles across the FSLWed AZ31B-H24 Mg alloy welds joined at (a) 1000 rpm and 20 mm/s, (b) 1500 rpm and 20 mm/s, and (c) 1500 rpm and 10 mm/s.

At a constant rotational rate of 1500 rpm, a decrease in the welding speed from 20 mm/s to 10 mm/s was observed to reduce the average hardness in the SZ slightly to roughly 52 HV (Figures 8(b) and (c)). At the lower welding speed of 10 mm/s, more heat may also be transported *via* conduction further into the weldment, as evidenced by the widening of the hardness trough (Figures 8(c) *vs* (b)). Moreover, the general micro-hardness profile along the top sheet of the lap welds was observed to have consistently lower hardness values than those along the bottom sheet, naturally due to the higher temperatures (and concomitantly a coarser grain structure) experienced locally in the upper workpiece during FSW, as corroborated previously.[26,27]

The effect of grain size on the hardness or strength of the AZ31B-H24 Mg alloy can be rationalized through a Hall–Petch-type relationship. Specifically, the finer grain size of the BM microstructure would exhibit a higher hardness value as compared to the progressively coars-ened grain structure from the HAZ (across the TMAZ) to the center of the SZ, since the grain boundaries are the major barrier to the slip of dislocations. Hence, the processes/welding conditions that result in coarser grains would have a lower resistance to localized plastic deformation (*i.e.*, fewer grain boundaries) and render a decrease in the hardness or strength. Figure 9 shows the relationship between the average hardness values mea-sured in the SZ and the average grain size determined in the SZ for the different welding conditions examined in the present work. It should be noted that the average grain size was assessed from approximately 4,000 grains in the SZ in each welding condition and about 10,000 grains in the BM. The Hall–Petch-type relation-ship obtained between the hardness and the grain size (*d*) in the SZ of the FSLWed AZ31B-H24 Mg alloy (Figure 9) could be expressed as

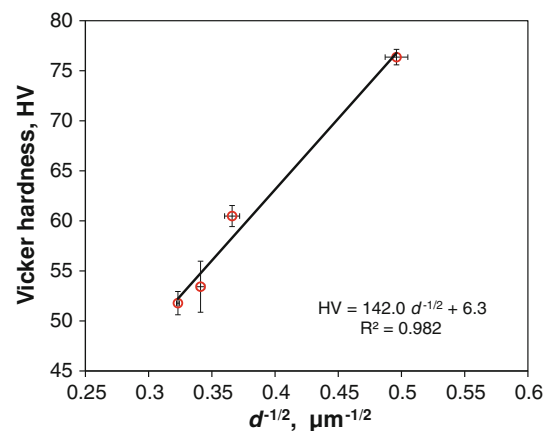$$\text{HV} = 142.0 d^{-\frac{1}{2}} + 6.3 \qquad [4]$$

Fig. 9—Hall-Petch-type relationship between the average hardness and average grain size in the SZ of the FSLWed AZ31B-H24 Mg al-loy weld joined with different welding parameters, where the BM grain size and hardness data are also plotted (The error bars on the plotted data represent the standard deviations for both hardness and grain size values.).

D. Fatigue Properties

Fatigue tests were performed to evaluate the strength of the FSLWed AZ31B-H24 Mg alloy in the tensile-
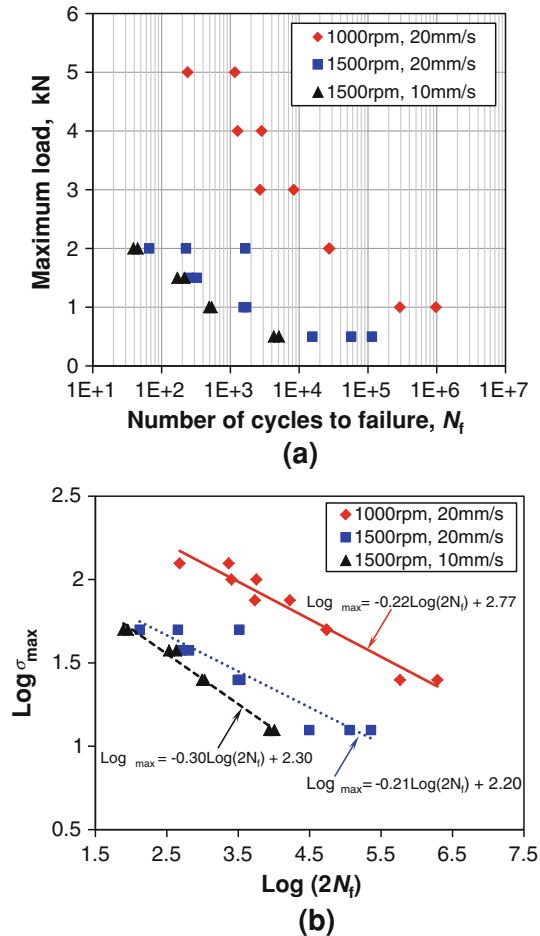

(a)

(b)

Fig. 10—Fatigue life curves of the friction stir lap welds manufactured with various rotational rates and welding speeds and tested at room temperature, $R = 0.2$, and 50 Hz: (a) Semi-log scale plot of the maximum load vs the number of cycles to failure (N_f) and (b) Double-log scale plot of the maximum stress vs the number of reversals to failure ($2N_f$).

shear configuration under cyclic loading (Figure 1(d)). The fatigue experimental data obtained at room temperature (RT), $R = 0.2$, and 50 Hz are plotted in Figure 10 in the form of the maximum load as a function of the number of cycles to failure for the lap welds assembled using various welding parameters, $i.e.$, tool rotational and welding speeds (1000 rpm and 20 mm/s, 1500 rpm and 20 mm/s, as well as 1500 rpm and 10 mm/s). It is seen from Figure 10(a) that at all load levels applied, the FSLWed AZ31B-H24 Mg alloy joints made with a welding condition of 1000 rpm and 20 mm/s had a much longer fatigue life than that of the other two welding conditions, namely 1500 rpm– 10 mm/s and 1500 rpm–20 mm/s. Also, increasing the welding speed from 10 mm/s to 20 mm/s at a constant tool rotational rate of 1500 rpm gave a visibly longer fatigue life for the maximum cyclic load ranging from 0.5 to 2 kN. This can be better observed from Figure 10(b) where the fatigue data are presented in a double-log scale of the maximum stress vs the number of reversals to failure ($2N_f$) for the FSLWed AZ31B-H24 Mg alloy joints assembled with the different welding conditions. It is clear that the fatigue life over the entire range from 1 kN to 5 kN was the longest for the welds joined at 1000 rpm and 20 mm/s, and the shortest for the welds joined at 1500 rpm and 10 mm/s, with the welds joined at 1500 rpm and 20 mm/s positioned in between those two lines. This was primarily attributed to the severity of welding defects (Figures 3 to 5) in conjunction with the microstructural changes (Figures 6 and 7).

For the lap joint configuration shown in Figure 1(d) used in the present study, the maximum stress occurs in the top workpiece on the AS and in the bottom workpiece on the RS, due to the stress distribution and the bending stresses present during fatigue testing, thereby representing the critical locations for fatigue crack initiation. In addition, the reorientation of the interface extends the hook into either the top or bottom workpiece, causing a net reduction in the EST of the material. The EST is defined as the minimum sheet thickness by measuring the smallest distance from any unbonded interface tip either to the top surface of the upper workpiece or to the bottom surface of the lower
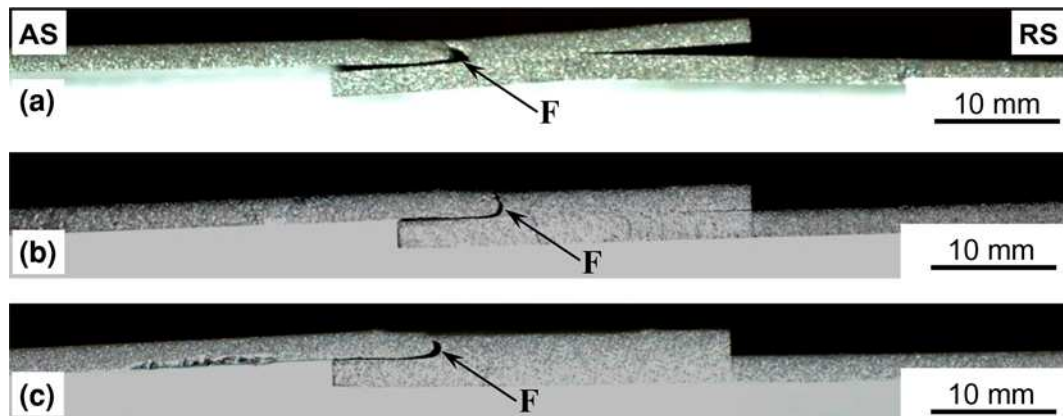

Fig. 11—Fatigue failure locations (as indicated by F) in the FSLWed AZ31B-H24 Mg alloy weld joined at the various tool rotational and welding speeds: (a) 1000 rpm, 20 mm/s, (b) 1500 rpm, 20 mm/s, and (c) 1500 rpm, 10 mm/s.

workpiece, whichever is smaller.[31,45] This parameter, introduced by Cederqvist and Reynolds,[46] may be used to measure the extent of how much of the original sheet thickness remains effectively capable of carrying the load after welding. Therefore, the thinning of the overlap sheets, caused by the hooking defect, is the primary cause for the reduction of fatigue life in FSLWed Al alloys.[17,31,47]

The fracture of the AZ31B-H24 Mg alloy lap welds was observed to occur predominantly in or near the interface of the SZ/TMAZ on the AS of the top workpiece (Figure 11), where the severe stress concentration arising from the presence of the hooking defect caused the crack to propagate directly into the top workpiece. In contrast, OJLwSPDs (Figure 5) were less damaging due to the fact that there were no sharp corners/edges for stress concentration. Additionally, there existed some mechanical bonding between the interfaces for OJLwSPD defects, which was not the case for the hooking defects. Therefore, hooking was the most damaging defect in the FSLWed joints. As mentioned earlier and shown in Figure 4(a), the welded joints made with the "hot" welding condition of 1500 rpm and 10 mm/s had the largest hooking height, resulting in the smallest EST or load-carrying capacity, and thus the shortest fatigue life (Figure 10). In contrast, the "cold" welding condition of 1000 rpm and 20 mm/s considerably suppressed the occurrence of the
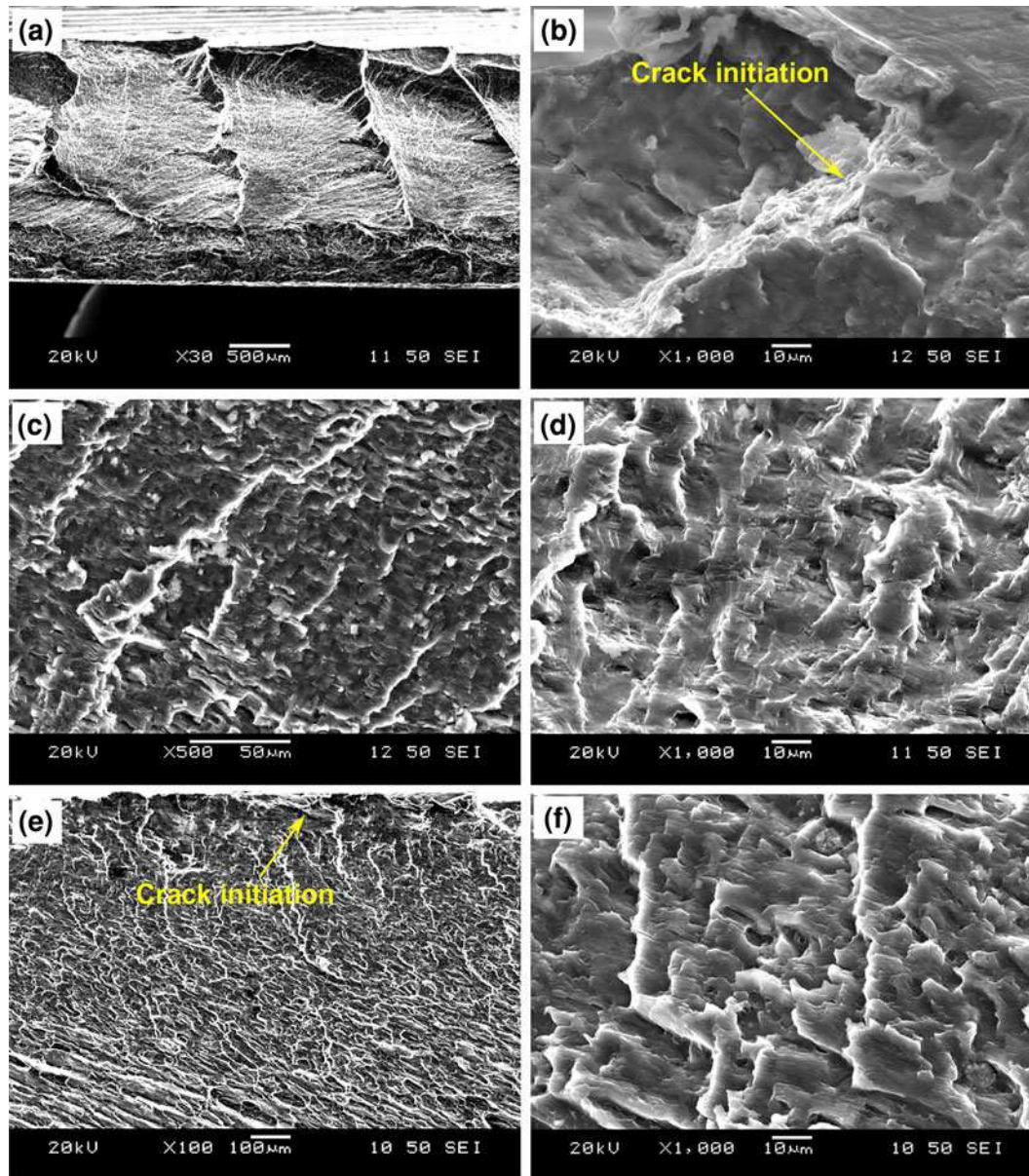

Fig. 12—Typical SEM images of the fatigue fracture surface of a FSLWed AZ31B-H24 Mg alloy assembled at a rotational rate of 1000 rpm and a welding speed of 20 mm/s: (a) fatigue fracture surface at a lower P_{max} = 1 kN, (b) crack initiation site at a lower P_{max} = 1 kN, (c) crack propagation region at a lower P_{max} = 1 kN, (d) fatigue striations at a higher magnification at a lower P_{max} = 1 kN, (e) fatigue fracture surface and crack initiation site at a higher P_{max} = 5 kN, and (f) crack propagation region at a higher P_{max} = 5 kN.

hook (Figures 4(e) and (f)), giving rise to the longest fatigue life (Figure 10).

E. *Fractography*

The fatigue tests showed that all the FSLWed specimens fractured near the interface of the SZ/TMAZ on the AS of the top workpiece. These fracture locations corresponded to the more critical hooking defects that resulted from excessive upward flow of the material and the occurrence of upper workpiece thinning during FSW (Figure 4). In particular, fatigue fracture was observed to initiate from the tip of the hooking defect lines due to the presence of severe stress concentration, and crack propagation occurred within the weld region, as indi-cated in Figure 11. Figures 12 to 14 show the SEM images of the fatigue fracture surface of the FSLWed AZ31B-H24 Mg alloy joints made with different welding parameters and tested at varying cyclic load levels. These fractographic images displayed several different zones, including fatigue crack initiation, propagation, and final rapid fracture. It can be observed that the fracture exhibited multiple crack initiations from the interior of the upper workpiece corresponding to the tip/root of the hooking defect, as shown in Figures 12(a) and (b). At a lower cyclic load level, fatigue cracking originated from the hook opening through the TMAZ and then propagating into the SZ, as indicated by arrows in Figures 12(b), 13(b), and 14(b). Fatigue crack propagation was mainly characterized by fatigue
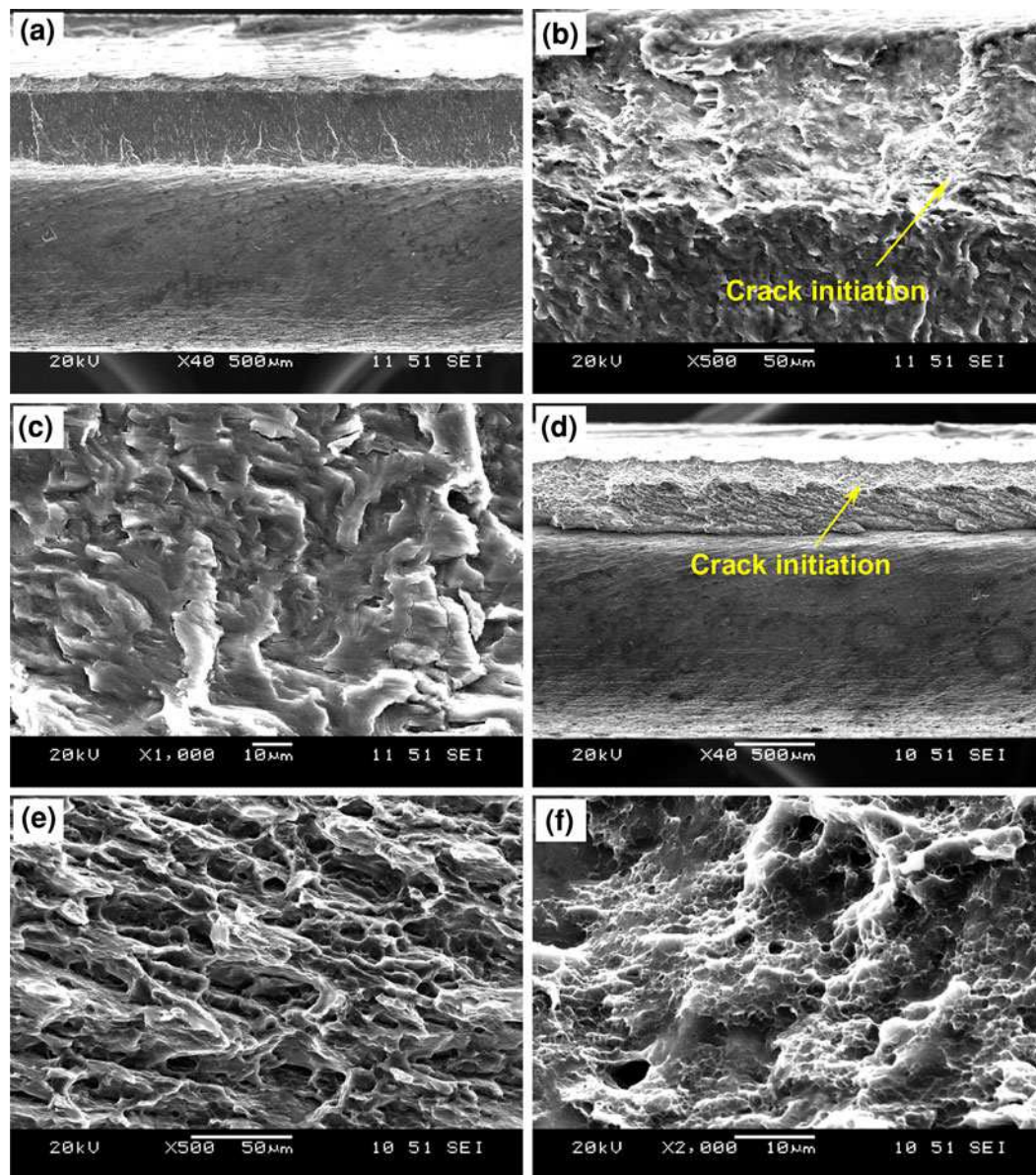

Fig. 13—Typical SEM images of the fatigue fracture surface of a FSLWed AZ31B-H24 Mg alloy assembled at a rotational rate of 1500 rpm and a welding speed of 10 mm/s: (*a*) fatigue fracture surface at a lower P_{max} = 0.5 kN, (*b*) crack initiation site at a lower P_{max} = 0.5 kN, (*c*) crack propagation region at a lower P_{max} = 0.5 kN, (*d*) fatigue fracture surface at a higher P_{max} = 2 kN, (*e*) crack propagation region at a higher P_{max} = 2 kN, and (*f*) crack propagation region at a further higher magnification at a higher P_{max} = 2 kN.
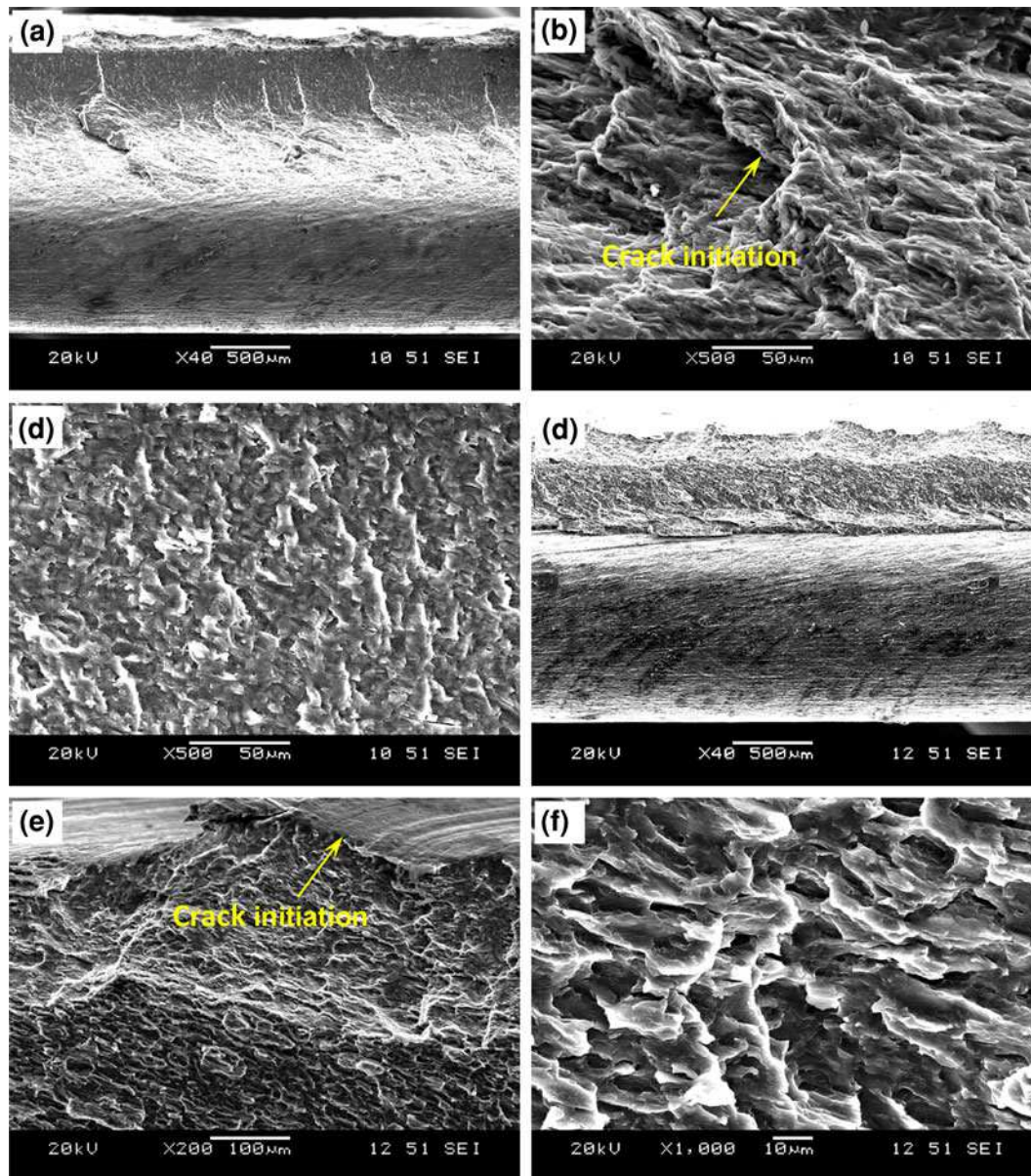
Fig. 14—Typical SEM images of the fatigue fracture surface of a FSLWed AZ31B-H24 Mg alloy assembled at a rotational rate of 1500 rpm and a welding speed of 20 mm/s: (*a*) fatigue fracture surface at a lower P_{max} = 0.5 kN, (*b*) crack initiation site at a lower P_{max} = 0.5 kN, (*c*) crack propagation region at a lower P_{max} = 0.5 kN, (*d*) fatigue fracture surface at a higher P_{max} = 2 kN, (*e*) crack initiation site at a higher P_{max} = 2 kN, and (*f*) crack propagation region at a further higher P_{max} = 2 kN.

striations (Figures 12(c) and (d), 13(c), and 14(c)) along with secondary cracks, which appeared usually perpendicular to the fatigue crack propagation direction. The fatigue striations, clearly observed at the higher magnifications, formed mainly by the repeated plastic blunting–sharpening process in the plastic zone ahead of a propagating crack arising from the twinning–detwinning process, which is reasonable considering the hexagonal close-packed crystal structure of the AZ31B-H24 Mg alloy in which there are a limited number of slip systems at room temperature.[48–50] At a higher cyclic load level, the crack also initiated in the region near the root of the hooking defects, indicated by the arrows in Figures 12(e), 13(d), and 14(e), and the propagation exhibited a mix of some dimples and cleavage-type fracture.

The final fracture surface appeared relatively coarser with the presence of plastic deformation and tearing ridge features.

IV. CONCLUSIONS

The influence of welding parameters, *i.e.*, tool rotational rate and welding speed, on the weld integrity of FSLWed AZ31B-H24 Mg alloy having a sheet thickness of 2 mm was examined. The following important conclusions could be drawn from this study:

1. The SZ and thermomechanically affected zone (TMAZ) experienced full dynamic recrystallization

and thus consisted predominantly of equiaxed grains. The grain size in the SZ increased with increasing heat input (*i.e.*, increasing tool rotational rate and decreasing welding speed).

2. The hardness decreased gradually from the BM through the HAZ, to the TMAZ, and then to the SZ where the lowest hardness was obtained. The overall hardness across the SZ was slightly higher at a lower heat input (*i.e.*, at a lower tool rotational rate and/or a higher welding speed).

3. The existence of hooking defects in friction stir lap welds was the key factor that significantly reduced the fatigue strength or life due to (i) the sharp tips causing severe stress concentration and (ii) the reduced EST (*i.e.*, large hooking height) or reduced load-bearing capacity. Specifically, the fatigue cracks usually initiated at the tip of the hooking defect on the AS of the top sheet due to the more severe stress concentration caused by the presence of a larger hook height. The fatigue crack then propagated into the SZ by the formation of fatigue striations perpendicular to the propagation direction, followed by the final rapid shear failure.

4. The welding parameters were observed to have a significant effect on the hook height and the subsequent fatigue life. A relatively "cold" weld conducted at a rotational rate of 1000 rpm and welding speed of 20 mm/s led to almost complete elimination of the hooking defect, thus considerably (over two orders of magnitude) improving the fatigue life.

5. Fractographic analysis revealed that the fracture surface exhibited multiple crack initiation sites originating from the tip of the hooking defect located in the upper workpiece. The crack propagation exhibited some more obvious brittle fracture features and was also differentiated by the characteristic fatigue striations.

REFERENCES

1. T.M. Pollock: *Science*, 2010, vol. 328, pp. 986–87.
2. M. Wise, K. Calvin, A. Thomson, L. Clarke, B. Bond-Lamberty, R. Sands, S.J. Smith, A. Janetos, and J. Edmonds: *Science*, 2009, vol. 324, pp. 1183–86.
3. D. Shindell, G. Faluvegi, M. Walsh, S.C. Anenberg, R.V. Dingenen, N.Z. Muller, J. Austin, D. Koch, and G. Milly: *Nat. Clim. Change*, 2011, vol. 1, pp. 59–66.
4. D.A. Howey: *Nat. Clim. Change*, 2012, vol. 2, pp. 28–29.
5. S.J. Davis, K. Caldeira, and H.D. Matthews: *Science*, 2010, vol. 329, pp. 1330–33.
6. J. Murray and D. King: *Nature*, 2012, vol. 481, pp. 433–35.
7. L.R. Kump: *Nature*, 2002, vol. 419, pp. 188–90.
8. W.M. Thomas, E.D. Nicholas, J.C. Needham, M.G. Church, P. Templesmith, and C.J. Dawes: GB Patent 9,125,978.9, 1991.
9. J.B. Jordon, J.B. Gibson, M.F. Horstemeyer, H.E. Kadiri, J.C. Baird, and A.A. Luo: *Mater. Sci. Eng. A*, 2011, vol. 528, pp. 6860–71.
10. Q. Yu, J. Zhang, Y. Jiang, and Q. Li: *Inter. J. Fatigue*, 2012, vol. 36, pp. 47–58.
11. S. Begum, D.L. Chen, S. Xu, and A.A. Luo: *Mater. Sci. Eng. A*, 2009, vol. A517, pp. 334–43.
12. H.Y. Wu, J.C. Yang, J.H. Liao, and F.J. Zhu: *Mater. Sci. Eng. A*, 2012, vol. 535, pp. 68–75.
13. H.Y. Wang, L.M. Liu, and Z.Y. Jia: *J. Mater. Sci.*, 2011, vol. 46, pp. 5534–40.
14. Q. Yu, J. Zhang, Y. Jiang, and Q. Li: *Int. J. Fatigue*, 2011, vol. 33, pp. 437–47.
15. C.L. Fan, D.L. Chen, and A.A. Luo: *Mater. Sci. Eng. A*, 2009, vol. A519, pp. 38–45.
16. X. Cao and M. Jahazi: *Mater. Des.*, 2009, vol. 30, pp. 2033–42.
17. D. Fersini and A. Pirondi: *Eng. Fract. Mech.*, 2007, vol. 74, pp. 468–80.
18. B.L. Mordike and T. Ebert: *Mater. Sci. Eng. A*, 2001, vol. 30, pp. 37–45.
19. W.R. Oates, eds.: *Welding Handbook, Materials and Applications*, pt. 1, vol. 3, 8th ed., American Welding Society, Miami, FL, 1996, pp. 121–62.
20. K.G. Watkins: *Magnesium Technology, Laser Welding of Magnesium Alloys*, H.I. Kaplan, ed., TMS, The Minerals, Metals & Materials Society, Warrendale, PA, 2003.
21. ASM International: *ASM Specialty Handbook, Magnesium and Magnesium Alloy*, ASM International, 1999, pp. 94–199.
22. H. Zhao and T. Debroy: *Welding Research Supplement*, August 2001, pp. 204s–210s.
23. B.A. Mickucki and J.D. Shearhouse: *Proceedings of Magnesium and Magnesium properties and Applications for Automobiles Conference*, SAE Inc., Detroit, 1993, pp. 107–15.
24. K.H. Leong, G. Kornecki, P.G. Sanders, and J.S. Keske: *Proceedings of ICALEO 1998*, Laser Institute of America, Orlando, 1998, Section F, pp 28–36.
25. H.B. Chen, K. Yan, T. Lin, S.B. Chen, C.Y. Jiang, and Y. Zhao: *Mater. Sci. Eng. A*, 2006, vol. 433, pp. 64–69.
26. R.S. Mishra and Z.Y. Ma: *Mater. Sci. Eng. R*, 2005, vol. 50, pp. 1–78.
27. M.W. Mahoney, C.G. Rhodes, J.G. Flintoff, R.A. Spurling, and W.H. Bingel: *Metall. Mater. Trans. A*, 1998, vol. 29A, pp. 1955–64.
28. X. Cao and M. Jahazi: *Proceedings of the 8th International Conference on "Trends in Welding Research"*, S.A. David, T. DebRoy, J.N. DuPont, T. Koseki, and H.B. Smart, eds., ASM International, Materials Park, OH, 2009.
29. Q. Yang, X. Li, K. Chen, and Y.J. Shi: *Mater. Sci. Eng. A*, 2011, vol. 528, pp. 2463–78.
30. G.M.D. Cantin, S.A. David, W.M. Thomas, E. Lara-Curzio, and S.S. Babu: *Sci. Technol. Weld Join.*, 2005, vol. 10, pp. 268–80.
31. M. Ericsson, L.Z. Jin, and R. Sandstrom: *Int. J. Fatigue*, 2007, vol. 29, pp. 57–68.

32. D. Fersini and A. Pirondi: *Eng. Fract. Mech.*, 2008, vol. 75, pp. 790–803.
33. ASTM International Standard ASTM D3164-03: "Standard test method for strength properties of adhesively bonded lap-shear sandwich joints in shear by tensile loading", 2003.
34. Y. Miyazaki and S. Furusako: *Nippon Steel Technical Report No.*, 2007, vol. 95, pp. 28–34.
35. Draft International Standard ISO/DIS 25239-1.2: Friction stir welding-aluminum-part 1, vocabulary, 2009.
36. S.M. Chowdhury, D.L. Chen, S.D. Bhole, and X. Cao: *Mater. Sci. Eng. A*, 2010, vol. 527 (21–22), pp. 6064–75.
37. T. Jene, G. Dobmann, G. Wagner, and D. Eifler: *Proceedings of the 6th International Symposium on Friction Stir Welding*, Montreal, Canada, 2006, pp. 1–6.
38. Y.S. Sato, F. Yamashita, Y. Sugiura, S.H.C. Park, and H. Kokawa: *Scripta Mater.*, 2004, vol. 50, pp. 365–69.
39. N. Afrin, D.L. Chen, X. Cao, and M. Jahazi: *Mater. Sci. Eng. A*, 2008, vol. 472, pp. 179–86.
40. S.H. Chowdhury, D.L. Chen, S.D. Bhole, X. Cao, and P. Wanjara: *Metall. Mater. Trans. A*, 2013, vol. 44A, pp. 323–36.
41. S.H. Chowdhury, D.L. Chen, S.D. Bhole, X. Cao, and P. Wanjara: *Mater. Sci. Eng. A*, 2012, vol. 556, pp. 500–509.
42. M. Fairman, N. Afrin, D.L. Chen, X.J. Cao, and M. Jahazi: *Can. Metall. Q.*, 2007, vol. 46, pp. 425–32.
43. O. Frigaard, O. Grong, and O.T. Midling: *Metall. Mater. Trans. A*, 2001, vol. 32A, pp. 1189–99.
44. Y.G. Kim, H. Fujji, T. Tsumura, T. Komazaki, and K. Nakata: *Mater. Sci. Eng. A*, 2006, vol. 415, pp. 250–54.
45. G.M. Cantin, S.A. David, E. Lara-Curzio, and S.S. Babu: *Proceedings of the 8th International Conference on "Trends in Welding Research"*, 2005, pp. 185–90.
46. L. Cederqvist and A.P. Reynolds: *Weld J. (Res. Supplement)*, 2001, vol. 12, pp. 281–87.
47. X. Xu, X. Yang, G. Zhou, and J. Tong: *Mater. Des.*, 2012, vol. 35, pp. 175–83.
48. C. Laird: *ASTM STP*, 1967, vol. 415, pp. 131–68.
49. S. Begum, D.L. Chen, S. Xu, and A.A. Luo: *Int. J. Fatigue*, 2009, vol. V31, pp. 726–35.
50. S. Begum, D.L. Chen, S. Xu, and A.A. Luo: *Metall. Mater. Trans. A*, 2008, vol. 39A, pp. 3014–26.